ACS Editors' Choice

JACS
JOURNAL OF THE AMERICAN CHEMICAL SOCIETY

Article

pubs.acs.org/JACS

Terms of Use

Untangling the Condensation Network of Organosiloxanes on Nanoparticles using 2D $^{29}Si-^{29}Si$ Solid-State NMR Enhanced by Dynamic Nuclear Polarization

Daniel Lee,[†,§] Guillaume Monin,[†,‡,∥,#] Nghia Tuan Duong,[†,§] Isabel Zamanillo Lopez,[†,‡,∥] Michel Bardet,[†,§] Vincent Mareau,[†,‡,∥] Laurent Gonon,[†,‡,∥] and Gaël De Paëpe*[,†,§]

[†]Univ. Grenoble Alpes, INAC, F-38000 Grenoble, France

[§]CEA, INAC, SCIB, F-38000 Grenoble, France

[‡]CEA, INAC, SPRAM, F-38000 Grenoble, France

[∥]CNRS, SPRAM, F-38000 Grenoble, France

Supporting Information

ABSTRACT: Silica (SiO_2) nanoparticles (NPs) were functionalized by silanization to produce a surface covered with organosiloxanes. Information about the surface coverage and the nature, if any, of organosiloxane polymerization, whether parallel or perpendicular to the surface, is highly desired. To this extent, two-dimensional homonuclear ^{29}Si solid-state NMR could be employed. However, owing to the sensitivity limitations associated with the low natural abundance (4.7%) of ^{29}Si and the difficulty and expense of isotopic labeling here, this technique would usually be deemed impracticable. Nevertheless, we show that recent developments in the field of dynamic nuclear polarization under magic angle spinning (MAS-DNP) could be used to dramatically increase the sensitivity of the NMR experiments, resulting in a timesaving factor of ~625 compared to conventional solid-state NMR. This allowed the acquisition of previously infeasible data. Using both through-space and through-bond 2D $^{29}Si-^{29}Si$ correlation experiments, it is shown that the required reaction conditions favor lateral polymerization and domain growth. Moreover, the natural abundance correlation experiments permitted the estimation of $^{2}J^{Si-O-Si}$-couplings (13.8 ± 1.4 Hz for surface silica) and interatomic distances (3.04 ± 0.08 Å for surface silica) since complications associated with many-spin systems and also sensitivity were avoided. The work detailed herein not only demonstrates the possibility of using MAS-DNP to greatly facilitate the acquisition of 2D $^{29}Si-^{29}Si$ correlation spectra but also shows that this technique can be used in a routine fashion to characterize surface grafting networks and gain structural constraints, which can be related to a system's chemical and physical properties.

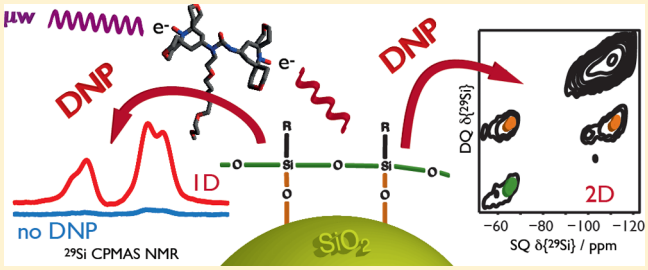

INTRODUCTION

Controlling surface- and self-condensation of functionalizing siloxanes is important to many research and technology fields. These siloxanes can be used to redesign surface properties, and as such, it is important to understand not only their reaction mechanisms and kinetics but also the dynamics of their self-assembly.[1] Specifically, silica (SiO_2) nanoparticles (NPs) can be grafted with siloxanes to obtain high surface area functional materials that have potential applications ranging from biomedicine (e.g., imaging, drug delivery, and contrast agents)[2] to industrial coatings.[3] However, the characterization of the coverage on these NPs can be difficult since conventional methods used for flat surfaces are not readily applicable.[4] Nevertheless, careful characterization is required and is of particular interest for our, and others', work on the development of proton exchange membrane fuel cells.

Proton exchange membrane fuel cells should be, in the near future, the best solution to produce clean electrical energy by converting the hydrogen chemical energy without the emission of pollutants. However, technological issues currently prohibit large-scale development. One of these issues is found at the heart of the device, in the polymer electrolyte of the membrane electrode assembly. Indeed, this membrane should operate at high temperature (100−150 °C) and therefore low relative humidity (10−50%) for both efficiency and lower catalyst poisoning.[5] Despite substantial research efforts, no current membrane offers good performance, in terms of both physical and chemical stability, at these specifications.[5,6]

An innovative strategy is to combine various approaches through the introduction of either functionalized silica NPs or a functionalized sol−gel network into the host ionomer. Functionalization is in the form of an organofunctional group capable of reducing the degrading species formed during fuel

Received: July 3, 2014
Published: August 25, 2014

   dx.doi.org/10.1021/ja506688m | J. Am. Chem. Soc. 2014, 136, 13781−13788

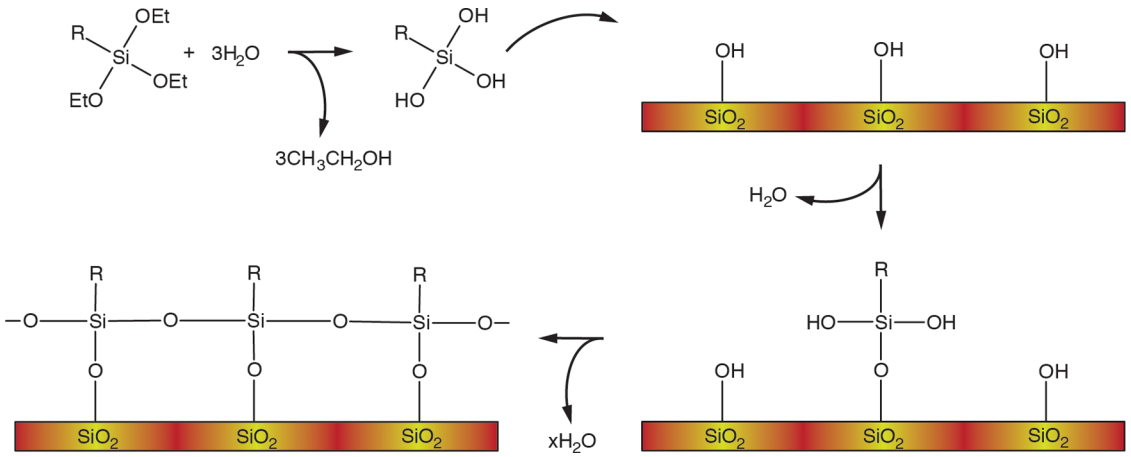

Figure 1. Illustration of lateral self-condensation of triethoxysilanes on a silica surface, eventually forming a perfectly condensed monolayer.

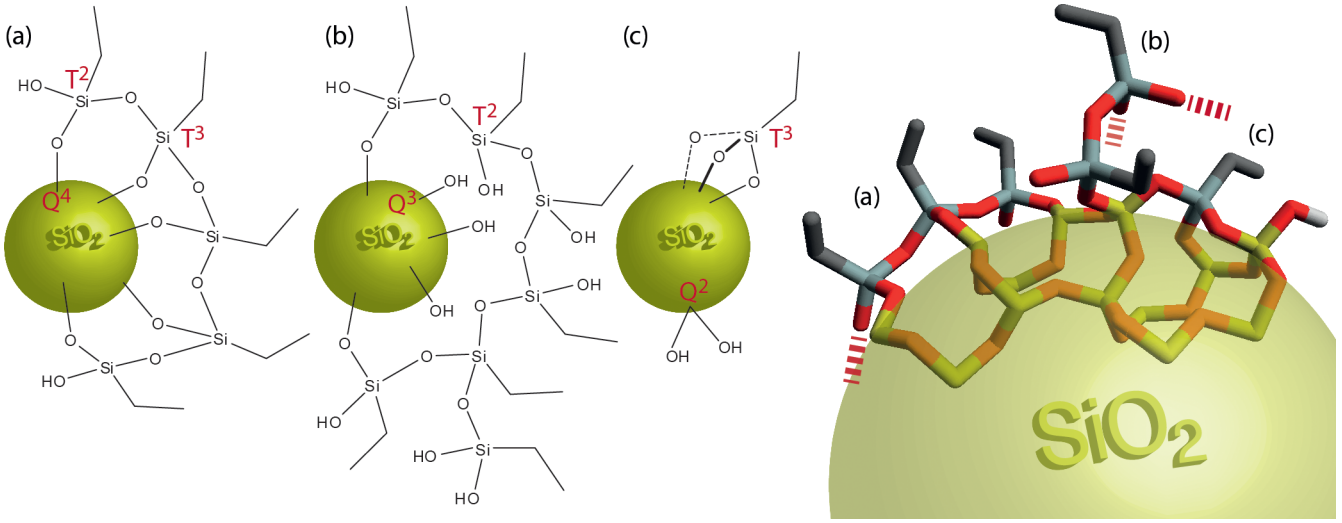

Figure 2. 2D (left) and 3D (right) schematics representing surface grafting possibilities for organosiloxanes on silica: (a) laterally self-condensed on the surface, (b) vertical core–shell oligomers above the surface, (c) discrete surface-bound monomers. The nanoparticle Si, silane Si, O, C, and H atomic environments are presented as yellow, light gray, red, dark gray, and white colors, respectively.

cell operation. In addition, these stabilizing sacrificial functions can be chosen to give new sulfonic acid groups once oxidized (thiols, disulfides, etc.),[7−11] therefore increasing the concentration of acid groups in the membrane and improving its proton conductivity. These hybrid membranes should then exhibit excellent chemical and thermomechanical stability, excellent water retention, and therefore excellent proton conduction at low relative humidity.

To avoid the elution of these stabilizing chemical functions in the water produced by the fuel cell (which would result in a loss of stabilizer or even in the poisoning of the electrodes' catalytic layers with sulfur stabilizing compounds),[12] these sacrificial sites should be perfectly immobilized in the membrane. Thus, the synthesis conditions must be carefully chosen to achieve the highest degree of condensation of the silanol groups of the sol–gel precursors used. Indeed, both the physical properties (proton conduction, thermomechanical stability) and durability of the obtained hybrid membrane strongly depend on the cross-linking density of the sol–gel network (i.e., the functionality of the precursors used, and the degree of condensation of the silanol functions). In the case of functionalized silica NPs, a perfectly condensed monolayer (see Figure 1) would be ideal as far as all stabilizing functions would be accessible to degrading agents and there would be no risk of eluting stabilizers. However, due to steric hindrance, the maximum theoretical surface coverage, defined in terms of reacted initial surface silanol sites, is expected to be <60% and depends on the size of the modifier molecule. The formation of a core–shell structure (forming a polymeric shell without condensation of organosiloxanes on the nanoparticle surface) could lead to the release of oligomers bearing unoxidized sulfur functions and therefore a potential poison for the electrodes' catalytic layers. Gaining an understanding of the extent of surface condensation on the silica NPs is therefore crucial to this work.

Solid-state NMR has been shown to be a powerful tool for the characterization of silica surfaces[13] and subsequent molecular grafting.[14] Mono- (M), di- (D), tri- (T), and quaternary- (Q) substituted silanes all have a particular chemical shift range in ^{29}Si NMR, and thus it is possible to assign NMR peaks in a corresponding spectrum to these structural details. It is also possible to obtain more intricacy and distinguish between different X^y sites, e.g., T^2 and T^3 sites (with y referring to the number of –O–Si bridges). However, these experiments generally require many hours of acquisition owing to the intrinsic sensitivity limitations of the technique, which is

dx.doi.org/10.1021/ja506688m | J. Am. Chem. Soc. 2014, 136, 13781−13788

further exacerbated by the small fraction of sample being studied (the surface). Furthermore, with the acquired spectra it is not possible to differentiate whether functionalizing silane molecules are mono-, di-, or tribound to the surface, core−shell above the surface, or laterally self-condensed on the surface. A schematic illustrating these different possibilities is given in Figure 2.

Recent technological advancements[15,16] have allowed for the efficient implementation of an approach that can alleviate the sensitivity limitations of solid-state NMR. Dynamic nuclear polarization (DNP) is an approach whereby the large polarization of unpaired electrons can be transferred to a nucleus or nuclei, thus dramatically increasing potential NMR sensitivity (theoretical maximum enhancement of ∼660 for protons).[17,18] Contemporary studies have only just started to demonstrate the subsequent accessible possibilities, which include, among others, selectively probing the surface of bacterial cells[19] as well as catalytic materials,[20,21] and the rapid characterization of pharmaceutical compounds[22] and organic polymers.[23,24] Furthermore, DNP-enhanced NMR has also been successfully applied to complex functionalized mesoporous silica systems[25,26] with resulting experimental time savings of several orders of magnitude.

Recently, we have demonstrated that it is possible to use DNP-enhanced solid-state NMR to record multidimensional spectra for various systems, which would have otherwise been infeasible.[21,27,28] It was shown that homonuclear carbon-13 proximities could be detected at natural isotopic abundance (1.1%) in minutes[27] to a few hours.[28] This highlighted the lack of the requirement for isotopic labeling for these studies. Silicon-29 has a natural isotopic abundance of ∼4.7%, and studies using isotopically enriched systems are very rare[29,30] owing to their great expense. Nevertheless, ^{29}Si-enriched tetraethyl orthosilicate (TEOS) is commercially available and can be an (expensive) interesting starting material when NMR characterization is desired. Compared to ^{13}C, the greater natural abundance of ^{29}Si can compensate for the intrinsic lower sensitivity and much smaller homonuclear coupling (cf. a dipolar coupling of ∼2200 Hz for nearest-neighbor ^{13}C nuclei in glycine and ∼170 Hz for nearest-neighbor ^{29}Si nuclei in silica), thus rendering natural abundance homonuclear correlation experiments more tenable using DNP-enhanced solid-state NMR. Although a few previous studies have shown these natural abundance correlation experiments are attainable with conventional solid-state NMR, they have been limited to silica samples with local crystallinity[31,32] and thus narrow (and accordingly intense) spectral lines. Furthermore, here one aims to study only the surface and not the entire material. Therefore, the sensitivity of any experiment will rely on the amount of surface, thus surface area of the system of interest, and the amorphous nature (spectral line widths) of the sample.

Here, we show that for a nanoparticulate silica system (diameter ∼10 nm, specific surface area ∼220 $m^2\ g^{-1}$) the interconnectivities of amorphous functionalizing polymers and/with the surface can be probed using 2D ^{29}Si−^{29}Si correlation NMR spectroscopy, enhanced by DNP. It is shown that for the employed reaction conditions the functionalizing siloxanes are successfully grafted to the surface of the silica NPs. Moreover, these siloxanes undergo self-condensation only on the surface and form clusters of reacted sites (leaving clusters of nonreacted sites). Finally, on account of the exceptional signal-to-noise achieved with DNP, structural parameters including bond lengths and *J*-couplings could be determined.

RESULTS AND DISCUSSION

Polyethylsiloxane- (PES-) functionalized silica NPs were synthesized as a model system using a dilute colloidal suspension protocol (see Experimental section) that avoids aggregation so that the NPs can then be evenly dispersed in the membrane ready for use in a fuel cell. Indeed, the amount of water present during a silanization reaction can be tuned to favor horizontal (lateral) or vertical self-condensation on the surface of the NPs.[1] However, from the reaction conditions required here (approximately 10 vol % water and 90 vol % *N*-methyl-2-pyrrolidone), it is not evident if the desired lateral surface condensation will be produced.

In preparation for the DNP experiments, 50 μL of a "DNP matrix" containing a glass-forming mixture of deuterated dimethyl sulfoxide ([$^2H_6$]DMSO), deuterated water (^2H_2O), and pure water (H_2O) (78, 14, 8 wt %, respectively) and 12 mM of the AMUPol[33] biradical polarizing agent was added to ∼50 mg of the dried functionalized silica nanopowder. The wetness-saturated mixture was stirred to allow for a more uniform coverage of the DNP matrix before being placed into a sapphire NMR rotor. This rotor was inserted into a probe suitable for magic angle spinning (MAS) and DNP and rotated at $\omega_r/(2\pi)$ = 5 kHz at a temperature of approximately 110 K. The low temperature is currently required for efficacy of DNP experiments and will perturb the dynamics of the system. However, the relevant chemical bonding will not be changed so low temperatures are fully applicable for this particular study. For DNP-enhanced NMR experiments the sample was irradiated with a few Watts of microwaves (μw) at a frequency optimized to drive the transfer of polarization using the cross effect (CE) DNP process[34,35] from electrons of nitroxide-based radicals to protons, approximately 263 GHz. For the experiments herein, the enhanced proton polarization was then transferred to ^{29}Si nuclei via a standard cross-polarization (CP) step.[36] Further details of the experimental conditions can be found in the Experimental section. The efficiency of the DNP process, ε_{DNP}, was determined by recording ^{29}Si CP spectra with and without μw irradiation and comparing the ratio of the signals. For the corresponding spectra of the PES-functionalized silica NPs shown in Figure 3, ε_{DNP} was 23 for the T sites ($\delta\{^{29}Si\}$ = −50 to −75 ppm) and 18 for the Q sites ($\delta\{^{29}Si\}$ = −90 to −115 ppm). The discrepancy between these two values most probably originates due to the existence of buried silanol ^{1}Hs in the bulk of the NPs.[37] These will not be hyperpolarized or will be hyperpolarized to a lesser extent compared to surface ^{1}Hs due to the much larger average distance from the polarizing

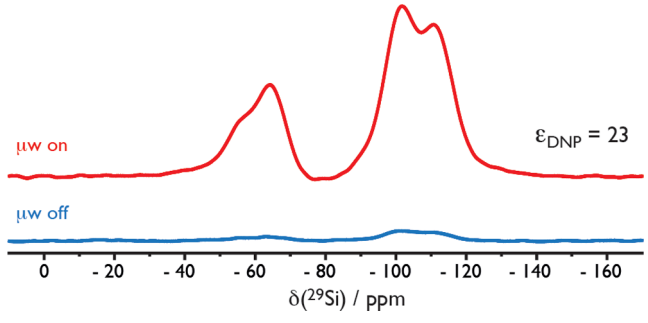

Figure 3. Illustration of the signal enhancement from DNP via 1D {^{1}H-}^{29}Si CPMAS spectra of the PES-functionalized silica NPs, recorded using conditions suitable for DNP with (red) and without (blue) microwave irradiation.

dx.doi.org/10.1021/ja506688m | J. Am. Chem. Soc. 2014, 136, 13781−13788

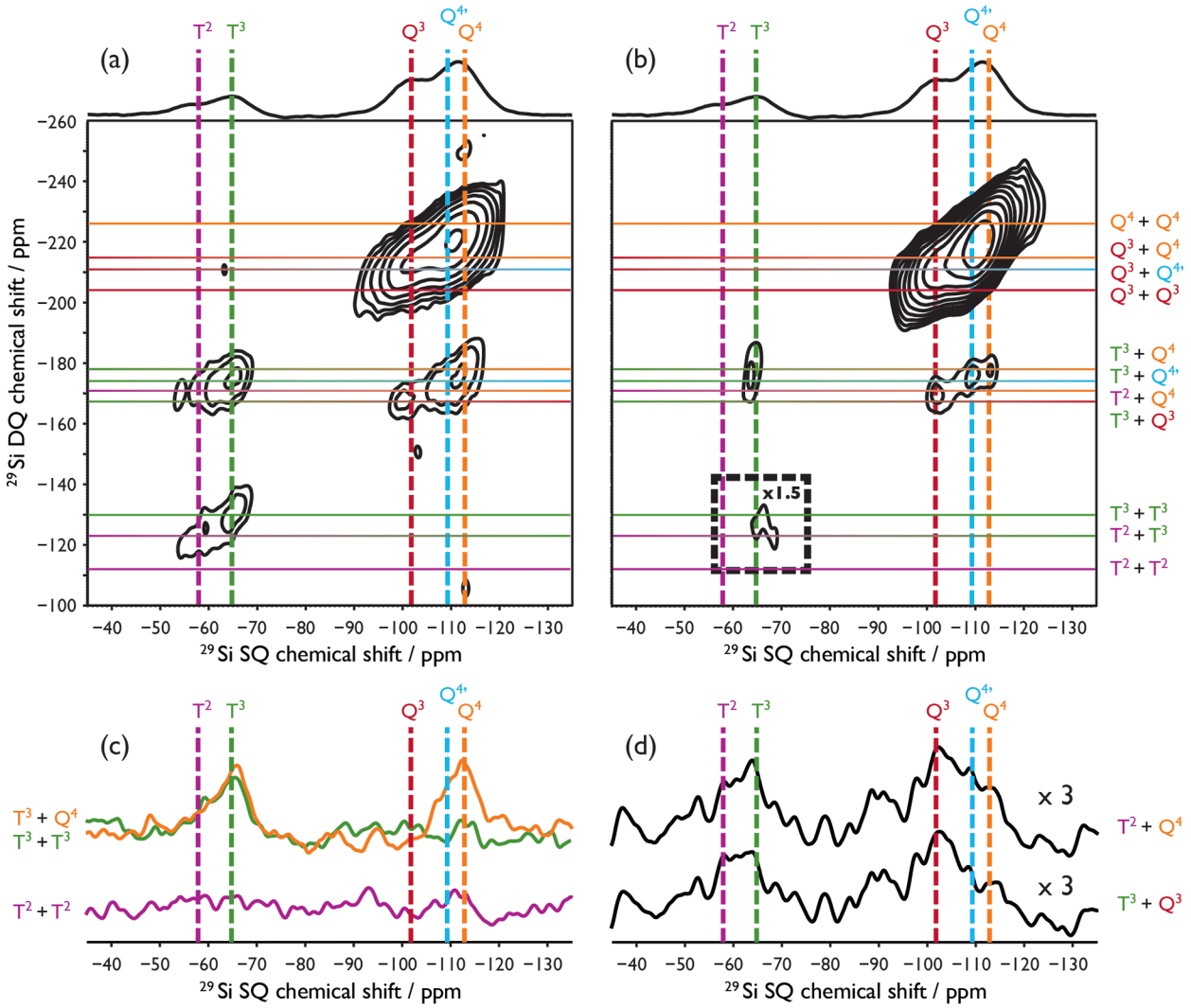

Figure 4. DNP-enhanced ^{29}Si–^{29}Si correlation spectra of the PES-functionalized silica NPs. Peaks are observed for resonances associated with silicon sites that share a through-space (a, c) or a through-bond (b, d) interaction with another silicon site. The nature of the peaks is further described in the text. Each 2D experiment was recorded in ∼5.5 h. Select cross sections through (a) and (b) are shown in (c) and (d), respectively. The region of the spectrum in (b) bordered by dashed lines has been magnified (×1.5) to demonstrate the presence of a low-intensity cross peak. Above each 2D spectrum, the 1D DNP-enhanced CPMAS spectrum from Figure 3, used for illustrative purposes.

agent and the lack of DNP-induced ^{1}H–^{1}H spin diffusion into the bulk NP and will therefore contribute to an overall smaller ε_{DNP} for Q species. Thus, ε_{DNP} can be used, cautiously, as an indirect proof of buried silanols. It is worth noting that other sample preparation procedures were tested but resulted in much smaller ε_{DNP}: ∼8 using the TOTAPOL biradical[38] in the same DNP matrix and ∼3 using the bCTbK biradical in 1,1,2,2-tetrachloroethane.[39] Presumably the smaller ε_{DNP} resulted from a less efficient polarizing agent for the former case and an unfavorable sample-solvent mixture for the latter.

Although ε_{DNP} is useful for determining the efficiency of the DNP process in a particular study, to examine the overall gain of implementing DNP when compared to conventional solid-state NMR experiments we have recently introduced the absolute sensitivity ratio (ASR).[27] This was introduced because there are more factors than simply ε_{DNP} that contribute to the overall signal of a DNP-enhanced experiment, some positively, some negatively. For example, two significant recent studies detail the increased NMR signal losses for MAS experiments as a result of the paramagnetic doping necessary for DNP.[40,41] Conventional signal "quenching" (removing beyond detection limits the amplitude of signals from nuclei close to the paramagnets) has been shown to increase dramatically under MAS.[40] Furthermore, the steady-state (microwave off) nuclear spin polarization can be reduced relative to its value at thermal equilibrium by the same mechanism that drives DNP in the manner here (the CE under MAS).[41] It should be highlighted that, for the latter case, a "more efficient" polarizing agent that gives a large ε_{DNP} may also lead to a greater perturbation of the steady-state polarization, resulting in a misleading ε_{DNP}. For the case here, the perturbation will lead to a decrease in the steady-state polarization and a larger ε_{DNP} than if the comparison was made to a system at thermal equilibrium. Accordingly, it is difficult to determine the efficacy of the DNP process in terms of overall NMR sensitivity.

The ASR is an experimentally determined parameter and compares the signal-to-noise per unit square root of time between experiments recorded under specific conditions required for DNP and under ubiquitous solid-state NMR conditions. Therefore, it intrinsically takes into account both

dx.doi.org/10.1021/ja506688m | J. Am. Chem. Soc. 2014, 136, 13781–13788

the positive and negative effects of the DNP conditions. Here, the ASR for the DNP-enhanced ^{29}Si CPMAS experiment of the functionalized NPs (compared to a room-temperature experiment using a fully packed 4 mm rotor, and thus ∼4 times the sample volume) was 25. This corresponds to an experimental timesaving factor of 625 (=ASR^2) by using DNP-enhanced NMR in the manner herein. The huge timesaving available through the application of DNP allowed the acquisition of 2D ^{29}Si homonuclear correlation experiments in a few hours (cf. ∼months, therefore infeasible, using conventional methods). Figure 4 shows two such correlation spectra, one (a) revealing spatial proximities (termed "through-space") and the other (b) highlighting through-bond connections. The pulse sequences used for these experiments are given in Figure S1. Note that ^{13}C experiments would be incapable of obtaining the information desired herein, irrespective of isotopic labeling.

For the through-bond (*J*-mediated) experiment the signal-to-noise obtained was ∼3.5 times smaller than for the through-space (dipolar-mediated) experiment due to the small coupling ($^2J^{\mathrm{Si-O-Si}}$ ∼ 5−15 Hz[30]) requiring long cross-peak build-up times (56 ms), which, when relaxation is considered (*vide infra*), results in approximately 2−3% transfer efficiency (cf. dipolar coupling of ∼170 Hz requiring 8 ms to transfer ∼8%). Despite the small transfer efficiency, the through-bond experiment was recorded to complement the through-space experiment. Silicon nuclei connected via a bridging oxygen atom have a spatial separation of approximately 3 Å. The nearest nonbonded silicon pairs can approach here is approximately 5 Å. Even in the absence of relaxation, the maximum transfer expected for this distance is approximately 1%, using the same through-space experimental conditions. Therefore, the through-space experiment shown here is anticipated to only show connections between bonded (via the bridging oxygen) silicon nuclei. Nevertheless, the through-bond experiment was performed for definitive evidence of direct connections between various ^{29}Si sites.

The correlation experiments used here will only produce peaks for coupled spin pairs (*i*,*j*). The peaks appear at the isotropic chemical shift (δ) of the individual spins in the horizontal dimension and at the sum of their combined chemical shifts in the vertical dimension, i.e. ($\delta_i + \delta_j$, δ_i) and ($\delta_i + \delta_j$, δ_j). Also shown in Figure 4c,d are various cross sections through the vertical dimension (of (a) and (b), respectively), further highlighting select correlations. It is clear from Figure 4 that there are many different types of coupled spins. As expected for the surface of a silica NP, there are Q^4−Q^4, Q^4−Q^3, and Q^3−Q^3 correlations. The pertinent information here is that, for these functionalized silica NPs, clusters of surface silanols are present (highlighted by the Q^3−Q^3 correlations).

For the siloxane part, T^3−Q^4 and T^2−Q^4 correlations are observed, which is proof of surface functionalization with the alkylsiloxane. Interestingly, a T^3−Q^3 correlation is also detected, which is direct evidence that these two species can be found bonded, via a bridging oxygen, at the surface. This is likely due to the condensation of an organosiloxane on a Q^2 site, with steric hindrance prohibiting further grafting onto the remaining silanol. Additionally, T^3−T^3 and T^3−T^2 correlations are observed, which demonstrates that the functionalizing siloxanes have undergone self-condensation and are bonded to each other. This could be interpreted as either self-condensation of the siloxane on the surface of the NPs (Figure 2a) or as the production of core−shell oligomers above the surface (Figure 2b). With similar signal intensity arising from T^3−Q^4 correlations as T^3−T^3 (see Figure 4c), it can be concluded that the T^3 sites, which are bonded to the surface, are also self-condensed on the surface. Therefore, there is a negligible amount of homopolymerization away from the surface. Similar correlation spectra showing a much greater intensity for T−T correlations compared to T−Q correlations would allude to a mainly core−shell system (Figure 2b). Conversely, spectra showing a much greater intensity for T−Q correlations compared to T−T correlations would imply a majority of discrete surface-bound monomers (Figure 2c). The existence of these discrete, surface-bound monomers cannot be comprehensively ruled out here since the intensity of the T−T correlations is slightly less than the T−Q correlations. However, slightly less intensity is expected since the signal from the T−T correlations will experience a more pronounced decay due to faster relaxation. This effect of faster relaxation for the T sites is particularly demonstrated in the through-bond experiment shown in Figure 4b, which shows nonsymmetrical "cross-peaks", i.e., the intensity at ($\delta_i + \delta_j$, δ_i) is different than that at ($\delta_i + \delta_j$, δ_j).

Two further interesting points can be drawn from the spectra shown in Figure 4. First, there is no evidence for T^2−T^2 connections (see Figure 4c). In the absence of homopolymerization away from the surface, these connections would signify self-condensed siloxane dimers attached to the surface. Due to the apparent large extent of surface self-condensation present here, the formation of these dimers is deemed unlikely. T^2 species then act like terminating "bookends" to self-condensed chains of T^3 species, as noted by the weaker T^2−T^3 and T^2−Q^4 correlations. This, along with the Q^3−Q^3 correlations (*vide supra*), suggests that the surface of the silica NPs is made up of clusters of self-condensed, surface grafted alkylsiloxanes and separate clusters of unreacted silanol groups. This indicates that the functionalization is not uniform on the surface and, consequently, that the silanization proceeds via nucleation and growth of functionalized domains. Furthermore, having clusters of unreacted silanols will be detrimental to desired functions for this type of system since these silanols will be less protected by the functionalizing siloxane and thus more accessible. The second point concerns the observation of correlations to a quaternary silicon site, here labeled $Q^{4\prime}$, that has an isotropic chemical shift 4 ppm more positive than the more prevalent, standard Q^4 site. Preliminary density functional theory (DFT) calculations (not shown) have suggested that this $Q^{4\prime}$ site resides on the surface of the silica NP and is directly bonded to the functionalizing siloxane. Further work is underway to obtain a more definitive assignment of this resonance. Nonetheless, this explanation would be consistent with the change in the Si−O−Si bond angles (related to the chemical shift)[30] anticipated for this silicon site as a result of the direct siloxane grafting.

Owing to the feasibility shown here of rapid collection of correlation data, further structural information can then be gained by performing an analysis on the experimental particulars. The transfer of magnetization between two coupled spins can be modeled and compared to experimentally determined "build-up curves", where the intensity of a correlation signal is measured as a function of the time allowed for the transfer (referred to as the "mixing time"). Usually, the analysis of build-up curves is complicated because the two coupled spins are not isolated from couplings to other spins. Here, the sensitivity achieved with the DNP allows this analysis to be performed using the low natural abundance of ^{29}Si (∼4.7%), which renders, on the basis of statistical probability,

dx.doi.org/10.1021/ja506688m | J. Am. Chem. Soc. 2014, 136, 13781−13788

the vast majority of spin-pairs isolated. For this reason, higher-order spin effects could be neglected here. For the through-bond experiment the maximum signal intensity for Q^4–Q^4 correlations was obtained at 56 ± 4 ms total mixing time (corresponding to 4τ in Figure S1). The time constant for the decay of the signal intensity during this experiment as a function of time, T_2', can be measured separately (using the pulse sequence shown in Figure S2). For the surface Q^4 sites, $T_2' \sim 15$ ms. Using the relation for the buildup of signal intensity in the presence of signal decay for this experiment:

$$\sin^2(2\pi/\tau)\cdot e^{-\tau/T_2'}$$

the J-coupling between surface Q^4 sites can be estimated as ${}^2J^{Si-O-Si} = 13.8 \pm 1.4$ Hz.

The simulated (using the SPINEVOLUTION program)[42] build-up curves for the through-space experiment fit the experimental data when assuming an interatomic distance of 3.04 ± 0.08 Å and a signal decay time constant of 7.5 ms. It is interesting to note that the time constant for the signal decay during the through-space experiment is exactly half that of the through-bond experiment. However, this could be expected since the through-bond experiment experiences decay of single quantum magnetization during the mixing periods, whereas the decay for the through-space experiment used here will be of double quantum magnetization, which can be twice as fast. Nevertheless, even accounting for the twice-as-fast observed signal decay, the much faster build up for the through-space experiment more than compensates and returns (3.5 times) more signal-to-noise here.

This information on the bond lengths and J-couplings is extremely relevant to structural studies. For instance, it has been shown that the magnitude of the J-coupling is proportional to the Si–O–Si bond angle.[30] The gathered information can then be used to apply constraints to theoretical models suitable for DFT calculations. In the opposite sense, DFT calculations can first be used to predict minimal energy (likely) structures and the corresponding NMR parameters.[43] The calculated NMR parameters, such as the J-coupling and chemical shift, can then be compared to experimental values, and thus the predicted structures can be screened. Furthermore, a more detailed evaluation can be achieved by simulating the build-up curves associated with each predicted structure and selecting those that differ least from the experimentally obtained curves.[32] However, as mentioned earlier, systems with many coupled spins pose problems for experimental build up curves owing to complex spin dynamics and lack of possible long-distance information (due to nearest-neighbor truncation). Therefore, dilute spin systems, such as ^{29}Si at natural abundance, are favored for structural studies if the sensitivity limitations are overcome.

CONCLUSION

Having sacrificial molecules able to reduce any degrading species formed during the operation of a proton exchange membrane fuel cell is highly desirable for the longevity of the device. The reaction conditions required to functionalize silica NPs that will eventually be dispersed in the membrane should then be optimized with respect to the final amount of accessible sacrificial sites while retaining a colloidal suspension. It has been shown that a relatively new technique, namely high-field DNP-enhanced solid-state NMR, can be used to determine whether the functionalization is in fact optimal. Surface coverage of functionalizing organosiloxanes can be examined through 2D ^{29}Si homonuclear correlation experiments that would be infeasible or impossible to acquire with conventional solid-state NMR due to the intrinsic sensitivity limitations (unless expensive and challenging isotopic labeling is employed). For PES-functionalized silica NPs, 2D data indicated that the employed reaction produced the favorable surface grafted, laterally self-condensed functionalizing groups without significant evidence for core–shell oligomers above the surface or discrete surface-bound monomers and that there were remaining clusters of silanol groups, which infers that the reaction proceeded via domain growth. This is true for the size of functionalizing molecule used here, whereas bulkier modifier molecules may produce different end results due to greater steric hindrance and changed reaction kinetics. As a bonus, structural parameters could be obtained due to the exceptional sensitivity of the experiments and the low natural isotopic abundance of the system used herein. The goal of the work was only to evaluate the condensation network at the surface of the NPs, but the availability of further structural information can lead to an improved understanding of the exact nature of the surface and consequently to progress in the design of functionalizing molecules in order to maximize required properties.

EXPERIMENTAL SECTION

Preparation of the PES-Functionalized Silica NPs. To prepare powerful mitigants of chemical degradation to be added to a polymer matrix in order to obtain hybrid membranes with improved lifetimes for fuel cell applications, a specific process has been developed. The objective was indeed to obtain high surface area functional NPs but also to avoid their aggregation before and after their dispersion into the polymer matrix. Functional NPs were thus prepared from commercial colloidal silica in water (Ludox HS 30, 30 wt % suspension, Sigma-Aldrich), *N*-methyl-2-pyrrolidone NMP (99.5% anhydrous, Sigma-Aldrich), and ethyl triethoxysilane (97%, Fluka), having in mind the importance of avoiding any dry step between NP functionalization and the preparation of hybrid membranes. To this extent, 10 mL of reactive solution was prepared by dilution of the ethyl triethoxysilane into NMP (final concentration: 0.1 M) before slowly adding 1 mL of the Ludox solution. The solution was kept at 100 °C for 3 h to reach an optimized functionalization of the silica NPs before rapid cooling to room temperature. The suspension of PES-functionalized NPs was purified by dialysis (membrane Membra-Cell, MD44, MWCO 14000) until there was a complete elution of the ungrafted organosilane. Specifically for the NMR experiments, functionalized NPs were obtained by solvent evaporation at 90 °C under argon followed by washing with pure water until the NMP was completely removed (evident through the NMR). For the DNP-enhanced NMR experiments, the PES-functionalized NPs were collected by centrifugation then dried under vacuum.

Standard Solid-State NMR Experiments. To acquire data to allow for the ASR measurement described in the text, a 4 mm rotor was filled with the pure PES-functionalized silica NPs, subsequently inserted into a probe suitable for double-resonance NMR and MAS and rotated at $\omega_r/2\pi = 5$ kHz under ambient conditions. The conventional SSNMR {^{1}H-}^{29}Si CPMAS experiments were performed on a Bruker AVANCE 400 MHz (9.4 T) spectrometer using the same pulse sequence timings and powers as for the experiments recorded under DNP conditions (*vide infra*) except that the experimental repetition delay was optimized as 1 s.

DNP-Enhanced Solid-State NMR Experiments. The ^2H_2O was purchased from Sigma-Aldrich and the [$^2H_6$]DMSO from VWR. Both were used without further purification. Prof. Paul Tordo and Dr Olivier Ouari from the Université d'Aix-Marseille are thanked for the donation of the AMUPol biradical. The experiments recorded under conditions suitable for DNP were performed on a Bruker DNP-

SSNMR AVANCE III 400 MHz spectrometer equipped with a gyrotron and transmission line capable of providing ∼5 W of 263 GHz microwave irradiation at the sample and a low-temperature 3.2 mm MAS probe suitable for spinning rates of up to 17 kHz and sample temperatures of ∼100 K.[16]

Experiments were acquired using a MAS rate of 5 kHz, ^{1}H $\pi/2$ pulses of 100 kHz, ^{29}Si $\pi/2$ and π pulses of 50 kHz, ^{29}Si CP pulses of ∼60 kHz applied for 3 ms (optimized for the T sites) with corresponding ramped (50−100%) ^{1}H CP pulses of ∼90 kHz. 100 kHz of SPINAL-64[44] heteronuclear decoupling was used throughout the 10 ms signal detection periods, which gave direct spectral widths of 50 kHz. These low-temperature (∼110 K) experiments used an optimized experimental repetition delay of 1.8 s. POST-C7[45] and refocused INADEQUATE[46] were used for the through-space (dipolar) and through-bond (*J*-) 2D homonuclear correlation experiments, respectively. The pulse sequences used for these experiments are given in Figure S1. The indirect dimensions used spectral widths of 17.5 kHz and total evolution times of 0.7 ms for the POST-C7 experiment and 0.4 ms for the refocused INADEQUATE. 1.7 times more transients were recorded for the refocused INADEQUATE (768 compared to 448), and *J*-evolution periods of 14 ms, combining for a total mixing time of 56 ms, were employed. The POST-C7 mixing time was 8 ms in total (4 ms each for excitation and reconversion). 100 kHz of SPINAL-64 decoupling was used throughout the indirect detection periods and also the *J*-evolution periods of the refocused INADEQUATE, whereas 130 kHz of CW Lee−Goldburg decoupling[47] was used during the POST-C7 mixing periods to best avoid interference with the recoupling sequence.

■ ASSOCIATED CONTENT

Supporting Information

NMR pulse sequences for the DNP-enhanced 2D homonuclear correlation experiments as well as the sequence used for the measurement of T_2' are given. This material is available free of charge via the Internet at http://pubs.acs.org.

■ AUTHOR INFORMATION

Corresponding Author

gael.depaepe@cea.fr

Present Address

[#]Guillaume Monin, Silvadec, PA de l'Estuaire 56190, Arzal, France.

Notes

The authors declare no competing financial interest.

■ ACKNOWLEDGMENTS

This work was supported by the French National Research Agency through the Labex ARCANE (ANR-11-LABX-0003-01), the "programme chaire d'excellence" (ANR08-CEXC-003-01), and the "programme blanc" (ANR-12-BS08-0016-01). The RTB and the Cluster MACODEV "Materials and Design for Sustainable Development" of the Rhône-Alpes regional Council are acknowledged for their financial support. D.L. was supported by CEA-EUROTALENTS (PCOFUND-GA-2008-228664) for part of the work.

■ REFERENCES

(1) Fadeev, A. Y.; McCarthy, T. J. *Langmuir* **2000**, *16*, 7268−7274.
(2) Piao, Y.; Burns, A.; Kim, J.; Wiesner, U.; Hyeon, T. *Adv. Funct. Mater.* **2008**, *18*, 3745−3758.
(3) Kotsuchibashi, Y.; Wang, Y.; Kim, Y.-J.; Ebara, M.; Aoyagi, T.; Narain, R. *ACS Appl. Mater. Interfaces* **2013**, *5*, 10004−10010.
(4) Brandriss, S.; Margel, S. *Langmuir* **1993**, *9*, 1232−1240.
(5) Borup, R.; Meyers, J.; Pivovar, B.; Kim, Y. S.; Mukundan, R.; Garland, N.; Myers, D.; Wilson, M.; Garzon, F.; Wood, D.; Zelenay, P.; More, K.; Stroh, K.; Zawodzinski, T.; Boncella, J.; McGrath, J. E.; Inaba, M.; Miyatake, K.; Hori, M.; Ota, K.; Ogumi, Z.; Miyata, S.; Nishikata, A.; Siroma, Z.; Uchimoto, Y.; Yasuda, K.; Kimijima, K.-I.; Iwashita, N. *Chem. Rev.* **2007**, *107*, 3904−3951.
(6) Kreuer, K. D. *J. Membr. Sci.* **2001**, *185*, 29−39.
(7) Koelewijn, P.; Berger, H. *Recl. Trav. Chim. Pays−Bas* **2010**, *93*, 63−68.
(8) Kúdelka, I.; Misro, P. K.; Pospíšil, J.; Korbanka, H.; Riedel, T.; Pfahler, G. *Polym. Degrad. Stab.* **1985**, *12*, 303−313.
(9) Kulich, D. M.; Reid Shelton, J. *Polym. Degrad. Stab.* **1991**, *33*, 397−410.
(10) Pobedimskii, D. G.; Buchachenko, A. L. *Bull. Acad. Sci. USSR, Div. Chem. Sci.* **1968**, *17*, 2579−2582.
(11) Richaud, E.; Monchy-Leroy, C.; Colin, X.; Audouin, L.; Verdu, J. *Polym. Degrad. Stab.* **2009**, *94*, 2004−2014.
(12) Barbier, J. In *Metal-Support and Metal-Additive Effects in Catalysis*; Imelik, B., Ed.; Elsevier Scientific Publishing Company: Amsterdam, 1982; pp 293−306.
(13) Maciel, G. E.; Sindorf, D. W. *J. Am. Chem. Soc.* **1980**, *102*, 7606−7607.
(14) Babonneau, F.; Baccile, N.; Laurent, G.; Maquet, J.; Azaïs, T.; Gervais, C.; Bonhomme, C. *C. R. Chim.* **2010**, *13*, 58−68.
(15) Barnes, a B.; Paëpe, G. De; van der Wel, P. C. a; Hu, K.-N.; Joo, C.-G.; Bajaj, V. S.; Mak-Jurkauskas, M. L.; Sirigiri, J. R.; Herzfeld, J.; Temkin, R. J.; Griffin, R. G. *Appl. Magn. Reson.* **2008**, *34*, 237−263.
(16) Rosay, M.; Tometich, L.; Pawsey, S.; Bader, R.; Schauwecker, R.; Blank, M.; Borchard, P. M.; Cauffman, S. R.; Felch, K. L.; Weber, R. T.; Temkin, R. J.; Griffin, R. G.; Maas, W. E. *Phys. Chem. Chem. Phys.* **2010**, *12*, 5850−5860.
(17) Overhauser, A. *Phys. Rev.* **1953**, *92*, 411−415.
(18) Carver, T. R.; Slichter, C. P. *Phys. Rev.* **1953**, *92*, 212−213.
(19) Takahashi, H.; Ayala, I.; Bardet, M.; De Paëpe, G.; Simorre, J.-P.; Hediger, S. *J. Am. Chem. Soc.* **2013**, *135*, 5105−5110.
(20) Vitzthum, V.; Miéville, P.; Carnevale, D.; Caporini, M. a; Gajan, D.; Copéret, C.; Lelli, M.; Zagdoun, A.; Rossini, A. J.; Lesage, A.; Emsley, L.; Bodenhausen, G. *Chem. Commun.* **2012**, *48*, 1988−1990.
(21) Lee, D.; Takahashi, H.; Thankamony, A. S. L.; Dacquin, J.; Bardet, M.; Lafon, O.; Paëpe, G. De. *J. Am. Chem. Soc.* **2012**, *134*, 18491−18494.
(22) Rossini, A. J.; Widdifield, C. M.; Zagdoun, A.; Lelli, M.; Schwarzwälder, M.; Copéret, C.; Lesage, A.; Emsley, L. *J. Am. Chem. Soc.* **2014**, *136*, 2324−2334.
(23) Blanc, F.; Chong, S. Y.; McDonald, T. O.; Adams, D. J.; Pawsey, S.; Caporini, M. A.; Cooper, A. I. *J. Am. Chem. Soc.* **2013**, *135*, 15290−15293.
(24) Ouari, O.; Phan, T.; Ziarelli, F.; Casano, G.; Aussenac, F.; Thureau, P.; Gigmes, D.; Tordo, P.; Viel, S. *ACS Macro Lett.* **2013**, *2*, 715−719.
(25) Lelli, M.; Gajan, D.; Lesage, A.; Caporini, M. A.; Vitzthum, V.; Miéville, P.; Héroguel, F.; Rascón, F.; Roussey, A.; Thieuleux, C.; Boualleg, M.; Veyre, L.; Bodenhausen, G.; Copéret, C.; Emsley, L. *J. Am. Chem. Soc.* **2011**, *133*, 2104−2107.
(26) Rossini, A. J.; Zagdoun, A.; Lelli, M.; Lesage, A.; Copéret, C.; Emsley, L. *Acc. Chem. Res.* **2013**, *46*, 1942−1951.
(27) Takahashi, H.; Lee, D.; Dubois, L.; Bardet, M.; Hediger, S.; De Paëpe, G. *Angew. Chem., Int. Ed.* **2012**, *51*, 11766−11769.
(28) Takahashi, H.; Viverge, B.; Lee, D.; Rannou, P.; De Paëpe, G. *Angew. Chem., Int. Ed.* **2013**, *52*, 6979−6982.
(29) Cadars, S.; Lesage, A.; Hedin, N.; Chmelka, B. F.; Emsley, L. *J. Phys. Chem. B* **2006**, *110*, 16982−16991.
(30) Florian, P.; Fayon, F.; Massiot, D. *J. Phys. Chem. C* **2009**, *113*, 2562−2572.
(31) Brouwer, D. H.; Kristiansen, P. E.; Fyfe, C. A.; Levitt, M. H. *J. Am. Chem. Soc.* **2005**, *127*, 542−543.
(32) Brouwer, D. H.; Cadars, S.; Eckert, J.; Liu, Z.; Terasaki, O.; Chmelka, B. F. *J. Am. Chem. Soc.* **2013**, *135*, 5641−5655.
(33) Sauvée, C.; Rosay, M.; Casano, G.; Aussenac, F.; Weber, R. T.; Ouari, O.; Tordo, P. *Angew. Chem., Int. Ed.* **2013**, *52*, 10858−10861.
(34) Mentink-Vigier, F.; Akbey, U.; Hovav, Y.; Vega, S.; Oschkinat, H.; Feintuch, A. *J. Magn. Reson.* **2012**, *224*, 13−21.

(35) Thurber, K. R.; Tycko, R. *J. Chem. Phys.* **2012**, *137*, 084508.
(36) Schaefer, J.; Stejskal, E. O. *J. Am. Chem. Soc.* **1976**, *98*, 1031−1032.
(37) Davydov, V. Y.; Kiselev, A. V.; Zhuravlev, L. T. *Trans. Faraday Soc.* **1964**, *60*, 2254−2264.
(38) Song, C.; Hu, K.-N.; Joo, C.-G.; Swager, T. M.; Griffin, R. G. *J. Am. Chem. Soc.* **2006**, *128*, 11385−11390.
(39) Zagdoun, A.; Casano, G.; Ouari, O.; Lapadula, G.; Rossini, A. J.; Lelli, M.; Baffert, M.; Gajan, D.; Veyre, L.; Maas, W. E.; Rosay, M.; Weber, R. T.; Thieuleux, C.; Coperet, C.; Lesage, A.; Tordo, P.; Emsley, L. *J. Am. Chem. Soc.* **2012**, *134*, 2284−2291.
(40) Corzilius, B.; Andreas, L. B.; Smith, A. A.; Ni, Q. Z.; Griffin, R. G. *J. Magn. Reson.* **2014**, *240*, 113−123.
(41) Thurber, K. R.; Tycko, R. *J. Chem. Phys.* **2014**, *140*, 184201.
(42) Veshtort, M.; Griffin, R. G. *J. Magn. Reson.* **2006**, *178*, 248−282.
(43) Charpentier, T. *Solid State Nucl. Magn. Reson.* **2011**, *40*, 1−20.
(44) Fung, B. M.; Khitrin, A. K.; Ermolaev, K. *J. Magn. Reson.* **2000**, *142*, 97−101.
(45) Hohwy, M.; Jakobsen, H. J.; Edén, M.; Levitt, M. H.; Nielsen, N. C. *J. Chem. Phys.* **1998**, *108*, 2686−2694.
(46) Lesage, A.; Bardet, M.; Emsley, L. *J. Am. Chem. Soc.* **1999**, *121*, 10987−10993.
(47) Lee, M.; Goldburg, W. *Phys. Rev.* **1965**, *140*, A1261−A1271.